Steel and Composite Structures, *Vol. 28, No. 3 (2018) 349-362*
DOI: https://doi.org/10.12989/scs.2018.28.3.349

Time-dependent creep analysis and life assessment of 304 L austenitic stainless steel thick pressurized truncated conical shells

Mosayeb Davoudi Kashkoli [1] and Mohammad Zamani Nejad [*2]

[1] *Department of Mechanical Engineering, Shahid Chamran University of Ahvaz, Ahvaz, Iran*
[2] *Department of Mechanical Engineering, Yasouj University, Yasouj, Iran*

(*Received February 23, 2018, Revised April 16, 2018, Accepted May 23, 2018*)

Abstract. This paper presents a semi-analytical solution for the creep analysis and life assessment of 304L austenitic stainless steel thick truncated conical shells using multilayered method based on the first order shear deformation theory (FSDT). The cone is subjected to the non-uniform internal pressure and temperature gradient. Damages are obtained in thick truncated conical shell using Robinson's linear life fraction damage rule, and time to rupture and remaining life assessment is determined by Larson-Miller Parameter (LMP). The creep response of the material is described by Norton's law. In the multilayer method, the truncated cone is divided into *n* homogeneous disks, and *n* sets of differential equations with constant coefficients. This set of equations is solved analytically by applying boundary and continuity conditions between the layers. The results obtained analytically have been compared with the numerical results of the finite element method. The results show that the multilayered method based on FSDT has an acceptable amount of accuracy when one wants to obtain radial displacement, radial, circumferential and shear stresses. It is shown that non-uniform pressure has significant influences on the creep damages and remaining life of the truncated cone.

Keywords: creep; thick truncated conical shells; life assessment; multilayered method; first order shear deformation theory (FSDT); Larson-Miller parameter (LMP)

1. Introduction

Generally, shells are curved structures which exhibit significant stiffness against forces and moments. Shells often used as the basic process component in various structural and engineering applications such as pressure vessels, military, aerospace and turbo machinery (Sofiyev *et al*. 2003). Scientists have paid an enormous amount of attention to shells, resulting in numerous theories about their behavior. Truncated conical shells have widely been applied in many fields such as space flight, rocket, aviation, and submarine technology (Nejad *et al*. 2014). In most of these applications, the cone has to operate under severe mechanical and thermal loads, causing significant creep and thus reducing its service life. The consequence of creep failure of a component in-use can be tragic and expensive. There are many cases of engineering disasters resulting in loss of life and property due to creep. Therefore, the analysis of creep deformations and prediction of strain rates and fracture time is very important in these applications.

The aim of ''creep modeling for structural analysis'' is the development of methods to predict time-dependent changes of stress and strain states in engineering structures up to the critical stage of creep rupture (Altenbach *et al*. 2008).

Shear deformation theory is a suitable method for the purpose of calculation of stresses and displacements in axisymmetric thick shells (Eipakchi *et al*. 2003, Ghannad *et al*. 2009, 2012a, b, Ghannad and Nejad 2010, Nejad *et al*. 2017, Van Dung and Chan 2017, Abdelaziz *et al*. 2017, Hachemi *et al*. 2017, Jandaghian and Rahmani 2017, Sekkal *et al*. 2017). This kind of structures, with different geometries, different loadings and different boundary conditions, with even variable pressure, could be more easily solved by this method (Ghannad *et al*. 2013). Making use of FSDT and plane elasticity theory (PET), thermo-elastic stresses in thick cylindrical and conical shells made of homogeneous and functionally graded materials (FGMs) under thermal loading have been analyzed extensively in the past years (Foroutan *et al*. 2012, Ghannad and Nejad 2013, Ghannad *et al*. 2013, Fatehi and Nejad 2014, Mehditabar *et al*. 2014, Nejad *et al*. 2014, 2015b, 2017, Ahmed and Wahab 2015, Jabbari *et al*. 2015, 2016, Nejad and Fatehi 2015, Mazarei *et al*. 2016, Afshin *et al*. 2017, Gharibi *et al*. 2017, Sofiyev *et al*. 2017, Sofiyev and Osmancelebioglu 2017, Sofiyev 2017, 2018a, b). Sofiyev (2018a, b) presented the buckling analysis of functionally graded materials (FGMs) sandwich truncated conical shells (STCSs) under hydrostatic pressure was solved using the modified form of FSDT. Most of these works show that the FSDT is a suitable method for elastic analysis of shells. Using Galerkin`s method, Sofiyev and Aksogan (2002) investigated the dynamic stability of an orthotropic elastic conical shell, with elasticity moduli and density varying in the thickness direction. In this paper, the shell is subject to a uniform external pressure which is a power function of

*Corresponding author, Associate Professor,
E-mail: m_zamani@yu.ac.ir; m.zamani.n@gmail.com

ISSN: 1229-9367 (Print), 1598-6233 (Online)

time.

Over the last years, creep stresses in FGM and homogeneous thick-walled pressure vessels under thermal loading have been analyzed extensively with regard to the elastic material behavior (Yang 2000, You *et al*. 2007, Loghman *et al*. 2010, 2011, Singh and Gupta 2010, Dai and Zheng 2012, Loghman and Moradi 2013, Fesharaki *et al*. 2014, Kashkoli and Nejad 2014, Nejad and Kashkoli 2014, Singh and Gupta 2014, Kashkoli and Nejad 2015, Nejad *et al*. 2015a, Dehghan *et al*. 2016, Kashkoli *et al*. 2017a, b, 2018, Pankaj Thakur *et al*. 2017). In most of these studies, Norton law has been used to obtain history of stresses and strains in pressure vessels. Over the years the simple Robinson's linear life-fraction rule (Robinson 1952) has been very useful in estimating creep life and damage under non-steady conditions of stress and/or temperature. Among the most important relationships presented by researchers for assessments of creep life, LMP is widely used (Nobakhti and Soltani 2014). The LMP describes the equivalence of time at temperature for a steel under the thermally activated creep process of stress rupture. It permits the calculation of the equivalent times necessary for stress rupture to occur at different temperatures.

As mentioned above, to the best of the authors' knowledge, no analytical study has been carried out to date on creep response of truncated conical shells based on FSDT. In this study, assuming that the creep response of the material is governed by Norton's law, a semi-analytical solution is presented for the calculation of stresses and displacements of thick-walled truncated conical shell made of 304 L austenitic stainless steel. The governing equations are based on FSDT that accounts for the transverse shear. The governing equations are derived, using minimum total potential energy principle. Robinson's linear life fraction damage rule has been used to predict the creep damage histories during the life of the cone and Larson-Miller Parameter (LMP) has been used to obtain creep remaining life assessment. The results obtained for stresses and displacements are validated using the finite element method (FEM). Good agreement is found between the results.

2. Problem formulation

2.1 Thermo-elastic governing equations

In the first-order shear deformation theory, the sections that are straight and perpendicular to the mid-plane remain straight but not necessarily perpendicular after deformation and loading. In this case, shear strains and stresses are taken into consideration. Geometry of a thick truncated cone with thickness h, and length L, is shown in Fig. 1. The clamped-clamped cone is subjected to non-uniform internal pressure P, and also a distributed temperature field due to a steady-state heat conduction from inner surface to outer surface of the cone.

In Fig. 1, the location of a typical point m, within the shell element may be determined by R and z, as

$$r = R + z \tag{1}$$

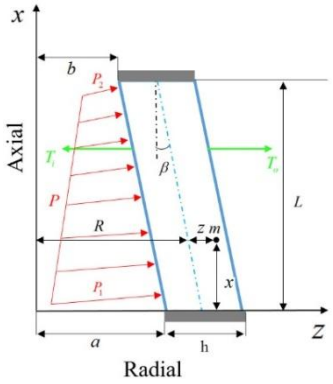

Fig. 1 Axial cross section of the thick truncated cone with clamped-clamped ends

where R represents the distance of middle surface from the axial direction, and z is the distance of typical point from the middle surface. In Eq. (1), x and z must be within the following ranges

$$-\frac{h}{2} \le z \le \frac{h}{2} \quad , \quad 0 \le x \le L \tag{2}$$

In Eq. (1), R is

$$R = a + \frac{h}{2} - x\tan(\beta) \tag{3}$$

where β is half of the taper angle as

$$\beta = \tan^{-1}\left((a-b)/L\right) \tag{4}$$

The general axisymmetric displacement field (U_x, U_θ, U_z), in the FSDT could be expressed on the basis of axial and radial displacements, as follow

$$\begin{cases} U_x(x,z) = u(x) + \phi(x)z \\ U_\theta(x,z) = 0 \\ U_z(x,z) = w(x) + \psi(x)z \end{cases} \tag{5}$$

where U_x, U_θ and U_z are displacement components along the axial, circumferential and radial directions. $u(x)$ and $w(x)$ are the displacement components of the middle surface. Also, $\phi(x)$ and $\psi(x)$ are unknown functions to determine the displacement field. The strain–displacement relations in the cylindrical coordinate system are

$$\begin{cases} \varepsilon_x = \dfrac{\partial U_x}{\partial x} = \dfrac{du(x)}{dx} + \dfrac{d\phi(x)}{dx}z \\ \varepsilon_\theta = \dfrac{U_z}{r} = \dfrac{1}{R+z}\left(w(x) + \psi(x)z\right) \\ \varepsilon_z = \dfrac{\partial U_z}{\partial z} = \psi(x) \\ \gamma_{xz} = \dfrac{\partial U_x}{\partial z} + \dfrac{\partial U_z}{\partial x} = \phi(x) + \left(\dfrac{dw(x)}{dx} + \dfrac{d\psi(x)}{dx}z\right) \end{cases} \tag{6}$$

In addition, the thermal stresses on the basis of constitutive equations for isotropic materials are as follow (Nejad *et al*. 2015b)

$$\begin{cases} \begin{Bmatrix} \sigma_x \\ \sigma_\theta \\ \sigma_z \end{Bmatrix} = \lambda E \begin{bmatrix} 1-\upsilon & \upsilon & \upsilon \\ \upsilon & 1-\upsilon & \upsilon \\ \upsilon & \upsilon & 1-\upsilon \end{bmatrix} \begin{Bmatrix} \varepsilon_x - \varepsilon_x^c \\ \varepsilon_\theta - \varepsilon_\theta^c \\ \varepsilon_z - \varepsilon_z^c \end{Bmatrix} \\ -\lambda E(1+\upsilon)\alpha_T T \begin{bmatrix} 1 \\ 1 \\ 1 \end{bmatrix} \\ \tau_{xz} = \lambda E\left(\frac{1-2\upsilon}{2}\right)\gamma_{xz} \\ \lambda = \frac{1}{(1+\upsilon)(1-2\upsilon)} \end{cases} \tag{7}$$

where T is temperature distribution and σ_i, ε_i and ε_i^c are the stresses, strains and creep strains in the axial, circumferential and radial directions, respectively. Also τ_{xz} and γ_{xz} are the shear stress and shear strain, respectively. In addition, υ, E and α_T are Poisson's ratio, modulus of elasticity and thermal expansion coefficient, respectively. The normal force per unit length (N_x, N_θ, N_z), bending moment per unit length (M_x, M_θ, M_z), shearing force per unit length (Q_x), and the twisting moment per unit length (M_{xz}) in terms of stress resultants are as

$$\begin{cases} \{N_x, N_\theta, N_z\} = \int_{-h/2}^{h/2} \left\{\sigma_x\left(1+\frac{z}{R}\right), \sigma_\theta, \sigma_z\left(1+\frac{z}{R}\right)\right\} dz \\ \{M_x, M_\theta, M_z\} = \int_{-h/2}^{h/2} \left\{\sigma_x\left(1+\frac{z}{R}\right), \sigma_\theta, \sigma_z\left(1+\frac{z}{R}\right)\right\} z dz \\ Q_x = K\int_{-h/2}^{h/2} \tau_{xz}\left(1+\frac{z}{R}\right) dz \\ M_{xz} = K\int_{-h/2}^{h/2} \tau_{xz}\left(1+\frac{z}{R}\right) z dz \end{cases} \tag{8}$$

where K is the shear correction factor that is embedded in the shear stress term. In the static state, for cylindrical shells, K = 5/6 (Vlachoutsis 1992).

On the basis of the principle of virtual work, the variations of strain energy are equal to the variations of the virtual work as follows

$$\delta U = \delta W \tag{9}$$

where U is the total strain energy of the elastic body and W is the total virtual work due to internal pressure. The strain energy is

$$\begin{cases} U = \iiint_V U^* dV \\ dV = r dr d\theta dx = (R+z) dx d\theta dz \\ U^* = \frac{1}{2}\left(\sigma_x \varepsilon_x + \sigma_\theta \varepsilon_\theta + \sigma_z \varepsilon_z + \tau_{xz}\gamma_{xz}\right) \end{cases} \tag{10}$$

The variation of the strain energy is

$$\delta U = \int_0^{2\pi}\int_0^{L}\int_{-h/2}^{h/2} \delta U^* (R+z)\, dz dx d\theta \tag{11}$$

The virtual work is

$$\begin{cases} W = \iint_S \left(\overrightarrow{f_{sf}} \cdot \vec{u}\right) dS \\ dS = r_i d\theta dx = \left(R - \frac{h}{2}\right) d\theta dx \\ \overrightarrow{f_{sf}} . \vec{u} = -PU_z \end{cases} \tag{12}$$

For axial distribution of internal pressure, the model of Eq. (13) is selected

$$P = P_1 + (P_2 - P_1)\left(\frac{x}{L}\right) \tag{13}$$

Here P_1 and P_2 are the values of pressure at the x = 0 and x = L, respectively. Applied pressure to inner surface includes two components as follows

$$P_x = P\sin(\beta) \quad , \quad P_z = P\cos(\beta) \tag{14}$$

Where P_x and P_z are components of internal pressure P along axial and radial directions, respectively. Thus, the variation of the virtual work is

$$\delta W = \int_0^{2\pi}\int_0^{L} \left(P_z \delta U_z + P_x \delta U_x\right)\left(R - \frac{h}{2}\right) dx d\theta \tag{15}$$

Substituting Eqs. (6) and (7) into Eqs. (11) and (15), and drawing upon calculus of variation and the virtual work principle (Eq. (9)), we will have

$$\begin{cases} \frac{d}{dx}(RN_x) = -P_x\left(R - \frac{h}{2}\right) \\ \frac{d}{dx}(RQ_x) - N_\theta = -P_z\left(R - \frac{h}{2}\right) \\ \frac{d}{dx}(RM_x) - RQ_x = P_x\frac{h}{2}\left(R - \frac{h}{2}\right) \\ \frac{d}{dx}(RM_{xz}) - M_\theta - RN_z = P_z\frac{h}{2}\left(R - \frac{h}{2}\right) \end{cases} \tag{16}$$

and the boundary conditions at the two ends of the cone are

$$\left[R\left(N_x\delta u + M_x\delta\phi + Q_x\delta w + M_{xz}\delta\psi\right)\right]_0^L = 0 \tag{17}$$

Substituting the stress components from Eqs. (7) into Eqs. (8) and then into the equilibrium equations (16), the following set of differential equation for displacement is obtained

$$\begin{cases} [B_1]\frac{d^2}{dx^2}\{y\} + [B_2]\frac{d}{dx}\{y\} + [B_3]\{y\} = \{F\} \\ \{y\} = \{du(x)/dx \quad \phi(x) \quad w(x) \quad \psi(x)\}^T \end{cases} \tag{18}$$

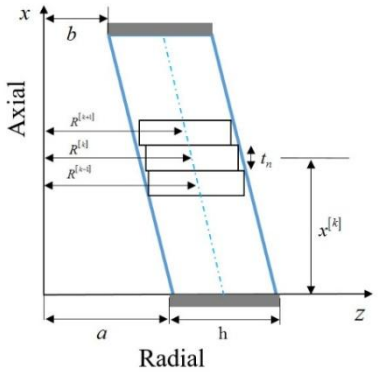

(a)

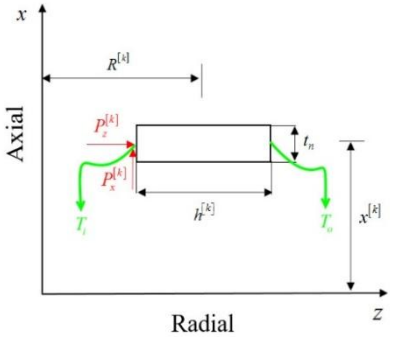

(b)

Fig. 2 (a) Division of thick truncated cone into homogenous disks with constant thickness; (b) Geometry of an arbitrary homogenous disk layer

where the coefficients matrices $[B_i]_{4\times4}$, and force vector $\{F\}_{4\times1}$ have been defined in the Appendix A.

2.1.1 Semi-analytical solution with multilayered method

Eq. (18) is the set of non-homogenous linear differential equations with variable coefficients. An analytical solution of this set of differential equations with variable coefficients seems to be difficult, if not impossible, to obtain. Hence, in the current study, a semi-analytical method for the solution of Eq. (18) is presented. In this method, the truncated cone is divided into homogenous disk layers with constant thickness t_n (Jabbari *et al*. 2016), (Fig. 2(a)).

Therefore, the governing equations convert to nonhomogeneous set of differential equations with constant coefficients. $x^{[k]}$ and $R^{[k]}$ are length and radius of middle of disks. The length of middle of an arbitrary disk (Fig. 2(b)) is as follows

$$\begin{cases} x^{[k]} = \left(k-\dfrac{1}{2}\right)\dfrac{L}{n_L} \\ \left(x^{[k]}-\dfrac{t}{2}\right) \le x \le \left(x^{[k]}+\dfrac{t}{2}\right) \\ t = \dfrac{L}{n_L} \end{cases} \tag{19}$$

where n_L is the number of disks and k is the corresponding number given to each disk. The radius of middle point of each disk is as follows

$$R^{[k]} = a + \frac{h^{[k]}}{2} - x^{[k]}\,tan(\beta) \tag{20}$$

Thus

$$\left(\frac{dR}{dx}\right)^{[k]} = \frac{dR^{[k]}}{dx^{[k]}} = -tan(\beta) \tag{21}$$

The terms of pressure applied to each disk are as follows

$$P_x^{[k]} = P^{[k]}\,sin(\beta) \quad , \quad P_z^{[k]} = P^{[k]}\,cos(\beta) \tag{22}$$

where

$$P^{[k]} = P_1 + \left(P_2 - P_1\right)\left(\frac{x^{[k]}}{L}\right) \tag{23}$$

Considering shear stress and based on FSDT, nonhomogeneous set of ordinary differential equations with constant coefficient of each disk is obtained as follows

$$\begin{cases} \left[B_1\right]^{[k]}\dfrac{d^2}{dx^2}\{y\}^{[k]} + \left[B_2\right]^{[k]}\dfrac{d}{dx}\{y\}^{[k]} + \left[B_3\right]^{[k]}\{y\}^{[k]} = \{F\}^{[k]} \\ \{y\}^{[k]} = \left\{du(x)^{[k]}/dx \quad \phi(x)^{[k]} \quad w(x)^{[k]} \quad \psi(x)^{[k]}\right\}^T \end{cases} \tag{24}$$

2.1.2 Heat conduction formulation

In the steady-state case and in the absence of heat generation, the heat conduction equation for the one-dimensional problem in polar coordinates simplifies to (Obata and Noda 1994)

$$\frac{d}{dr}\left[k_T\, r\frac{dT}{dr}\right] = 0 \tag{25}$$

where k_T is thermal conductivity of the cone. By considering $r = R + z$, Eq. (25) can be written as follows

$$\frac{d}{dz}\left[k_T^{[k]}\left(R^{[k]}+z\right)\frac{dT^{[k]}}{dz}\right] = 0 \tag{26}$$

Solving the differential Eq. (26), finally the terms of temperature gradient are derived as follows

$$T^{[k]} = g_1^{[k]}\int\frac{dz}{k_T^{[k]}\left(R^{[k]}+z\right)} + g_2^{[k]} - T_{ref} \tag{27}$$

where $g_1^{[k]}$ and $g_2^{[k]}$ are constants of integration which obtained from boundary conditions (See Appendix B). T_{ref} is the reference temperature where in this study assumed that $T_{ref} = T_o$. If the prescribed surface temperature imposed on inner and outer surfaces of the cone, temperature

gradient distribution is obtained as

$$T^{[k]}=\left(T_o-T_i\right)\left(\left[\frac{ln\left(\dfrac{R^{[k]}+z}{R^{[k]}-h^{[k]}/2}\right)}{ln\left(\dfrac{R^{[k]}+h^{[k]}/2}{R^{[k]}-h^{[k]}/2}\right)}\right]-1\right) \tag{28}$$

2.1.3 Thermo-elastic solution

For thermo-elastic analysis of thick truncated cone the creep strains ($\varepsilon_x^c,\ \varepsilon_\theta^c,\ \varepsilon_z^c$) are ignored. The total solution for Eq. (24) is

$$\{y\}^{[k]}=\sum_{i=1}^{6}C_i^{[k]}\{V\}_i^{[k]}e^{m_i^{[k]}x}+\left[B_3^{[k]}\right]^{-1}\{F\}^{[k]} \tag{29}$$

where C_i are unknown values and may be determined from boundary and continuity conditions. In addition, m_i and $\{V\}_i$ are eigenvalues and eigenvectors, respectively.

2.1.4 Boundary and continuity conditions

Given that the two ends of the cone are clamped, then

$$\begin{Bmatrix}U_x(x,z)\\U_z(x,z)\end{Bmatrix}_{x=0,L}=\begin{Bmatrix}0\\0\end{Bmatrix} \tag{30}$$

Because of continuity and homogeneity of the cone, at the boundary between two layers, forces, stresses and displacements must be continuous. Given that shear deformation theory applied is an approximation of one-order and also all equations related to the stresses include the first derivatives of displacement, the continuity conditions are as follows

$$\begin{aligned}
&\begin{Bmatrix}U_x^{[k-1]}(x,z)\\U_z^{[k-1]}(x,z)\end{Bmatrix}_{x=x^{[k-1]}+t/2}=\begin{Bmatrix}U_x^{[k]}(x,z)\\U_z^{[k]}(x,z)\end{Bmatrix}_{x=x^{[k]}-t/2}\\
&\begin{Bmatrix}\dfrac{dU_x^{[k-1]}(x,z)}{dx}\\\dfrac{dU_z^{[k-1]}(x,z)}{dx}\end{Bmatrix}_{x=x^{[k-1]}+t/2}=\begin{Bmatrix}\dfrac{dU_x^{[k]}(x,z)}{dx}\\\dfrac{dU_z^{[k]}(x,z)}{dx}\end{Bmatrix}_{x=x^{[k]}-t/2}\\
&\begin{Bmatrix}U_x^{[k]}(x,z)\\U_z^{[k]}(x,z)\end{Bmatrix}_{x=x^{[k]}+t/2}=\begin{Bmatrix}U_x^{[k+1]}(x,z)\\U_z^{[k+1]}(x,z)\end{Bmatrix}_{x=x^{[k+1]}-t/2}\\
&\begin{Bmatrix}\dfrac{dU_x^{[k]}(x,z)}{dx}\\\dfrac{dU_z^{[k]}(x,z)}{dx}\end{Bmatrix}_{x=x^{[k]}+t/2}=\begin{Bmatrix}\dfrac{dU_x^{[k+1]}(x,z)}{dx}\\\dfrac{dU_z^{[k+1]}(x,z)}{dx}\end{Bmatrix}_{x=x^{[k+1]}-t/2}
\end{aligned} \tag{31}$$

2.2 Governing equations for creep

For isotropic cone with creep behavior, the relations between rates of stress and strain are

$$\begin{cases}\begin{Bmatrix}\dot\sigma_x\\\dot\sigma_\theta\\\dot\sigma_z\end{Bmatrix}=\lambda E\begin{bmatrix}1-\upsilon&\upsilon&\upsilon\\\upsilon&1-\upsilon&\upsilon\\\upsilon&\upsilon&1-\upsilon\end{bmatrix}\begin{Bmatrix}\dot\varepsilon_x-\dot\varepsilon_x^c\\\dot\varepsilon_\theta-\dot\varepsilon_\theta^c\\\dot\varepsilon_z-\dot\varepsilon_z^c\end{Bmatrix}\\ \dot\tau_{xz}=\lambda E\left(\dfrac{1-2\upsilon}{2}\right)\dot\gamma_{xz}\end{cases} \tag{32}$$

where $\dot\sigma_i$, $\dot\varepsilon_i$ and $\dot\varepsilon_i^c$ are stress rates, strain rates and the creep strain rates in the axial, circumferential and radial directions, respectively. In addition, $\dot\tau_{xz}$ and $\dot\gamma_{xz}$ are the shear stress rate and shear strain rate, respectively. Creep strain rates are related to the stresses and the material uniaxial creep constitutive model by the well known Prandtle-Reuss equations as (Loghman *et al*. 2010)

$$\begin{Bmatrix}\dot\varepsilon_x^c\\\dot\varepsilon_\theta^c\\\dot\varepsilon_z^c\end{Bmatrix}=\frac{\dot\varepsilon_e^c}{\sigma_e}\begin{bmatrix}2&-1&-1\\-1&2&-1\\-1&-1&2\end{bmatrix}\begin{Bmatrix}\sigma_x\\\sigma_\theta\\\sigma_z\end{Bmatrix} \tag{33}$$

Where, $\dot\varepsilon_e^c$ and σ_e are the effective strain rate and effective stress, respectively. The Norton's creep constitutive model for the effective strain rate is (Loghman *et al*. 2010)

$$\dot\varepsilon_e^c=A\sigma_e^n \tag{34}$$

Substituting the Norton's law into Prandtle-Reuss equations, the relations between rates of creep strain and stresses may be as

$$\begin{cases}\begin{Bmatrix}\dot\varepsilon_x^c\\\dot\varepsilon_\theta^c\\\dot\varepsilon_z^c\end{Bmatrix}=\dfrac{A\sigma_e^{(n-1)}}{2}\begin{bmatrix}2&-1&-1\\-1&2&-1\\-1&-1&2\end{bmatrix}\begin{Bmatrix}\sigma_x\\\sigma_\theta\\\sigma_z\end{Bmatrix}\\ \sigma_e=\dfrac{1}{\sqrt{2}}\sqrt{\left(\sigma_x-\sigma_\theta\right)^2+\left(\sigma_x-\sigma_z\right)^2+\left(\sigma_z-\sigma_\theta\right)^2+6{\tau_{xz}}^2}\end{cases} \tag{35}$$

where A and n are material constants for creep. Using Eq. (16) and considering the pressure to be constant with time, the equilibrium equation for creep analysis is

$$\begin{cases}\dfrac{d}{dx}\left(R\dot N_x\right)=0\\ \dfrac{d}{dx}\left(R\dot Q_x\right)-\dot N_\theta=0\\ \dfrac{d}{dx}\left(R\dot M_x\right)-R\dot Q_x=0\\ \dfrac{d}{dx}\left(R\dot M_{xz}\right)-\dot M_\theta-R\dot N_z=0\end{cases} \tag{36}$$

Considering the temperature field to be steady, the following set of differential equations for displacement rates is obtained as follows

$$\begin{aligned}&\left[B_1\right]\frac{d^2}{dx^2}\{\dot y\}+\left[B_2\right]\frac{d}{dx}\{\dot y\}+\left[B_3\right]\{\dot y\}=\{F_c\}\\ &\{\dot y\}=\left\{d\dot u(x)/dx\quad\dot\phi(x)\quad\dot w(x)\quad\dot\psi(x)\right\}^T\end{aligned} \tag{37}$$

where the force vector $\{F_c\}_{4\times1}$ has been defined in the Appendix C.

2.2.1 Solution for creep

The total solution for Eq. (37) is

$$\{\dot{y}\}^{[k]} = \sum_{i=1}^{6} D_i^{[k]} \{V\}_i^{[k]} e^{m_i^{[k]}x} + \left[B_3^{[k]}\right]^{-1} \{F_c\}^{[k]} \quad (38)$$

where D_i are unknown values. When the stress rate is known, the calculation of stresses at any time t_i should be performed iteratively (Yang 2000)

$$\begin{cases} \sigma_{ij}^{(i)}(r,t_i) = \sigma_{ij}^{(i-1)}(r,t_{i-1}) + \dot{\sigma}_{ij}^{(i)}(r,t_i)\,dt^{(i)} \\ t_i = \sum_{k=0}^{i} dt^{(k)} \end{cases} \quad (39)$$

The solution of $t_i = 0$ corresponds to that for thermo-elastic material behavior. To calculate $\dot{\sigma}_{ij}^{(i)}(r,t_i)$, the stresses at the time t_{i-1} used.

3. Creep life assessment

The most used method for creep damage calculating is Robinson's linear life-fraction rule. According to this method, the fracture under variable load and temperatures can be predicted adding the creep life fractions consumed at each condition until their sum reaches the value of unity. The calculation of accumulated creep damage is performed at the end of each time increment Δt^i by using the following equation

$$D_f^i = \sum_{i=1}^{n} \frac{\Delta t^i}{t_r^i} \quad (40)$$

where D_f^i is creep damage and t_r^i is the creep fracture time at *i-th* time increment and at the equivalent stress and temperature of that point in the radial direction of the truncated cone. At rupture, $D_f^i = 1$, which is the rupture criteria. The time to rupture is calculated using LMP.

In contrast to the conventional creep tests, which take a long time, the LMP can be obtained using some sort of quick tests at high temperature and stress level and then extrapolating the results for prediction of the required parameters. The LMP is a grouping concept between rupture time (t_r) and temperature (T) for a particular stress level (Tahami *et al*. 2010). The Larson-Miller extrapolation parameter is in the following form

$$P_{L-M} = T.\left(C + log_{10}(t_r)\right) \quad (41)$$

In this equation T is in Kelvin, t_r is rupture time in hours and C is a physical parameter which has been assumed to be 20. This value is an accepted amount for most engineering materials and steels (Larson and Miller 1952) and therefore, has been used in this study to estimate the creep behaviour of the material. The LMP can be easily used to creep fracture data extrapolation, in which for any constant stress

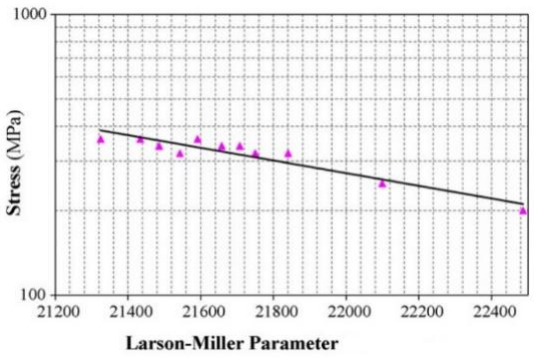

Fig. 3 Variation of stress versus Larson–Miller parameter for the 304L SS (Tahami *et al*. 2010)

level the combination of rupture time and test temperature, the LMP will remain constant (Tahami *et al*. 2010). The LMP variation with stress is shown in Fig. 3. The remaining life at any point in the radial direction of the truncated cone is then given by

$$RL^i = \left(1 - D_f^i\right) t_r^i \quad (42)$$

4. Numerical results and discussion

In this section, numerical results are presented and discussed for verifying the accuracy of the present theory in

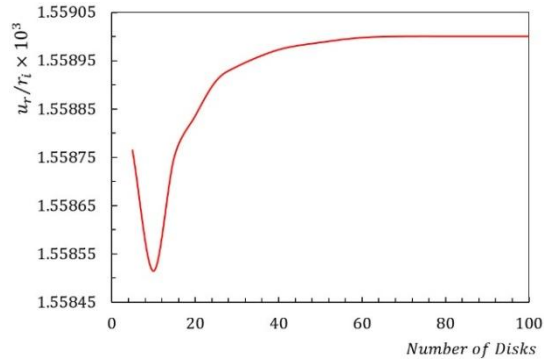

(a)

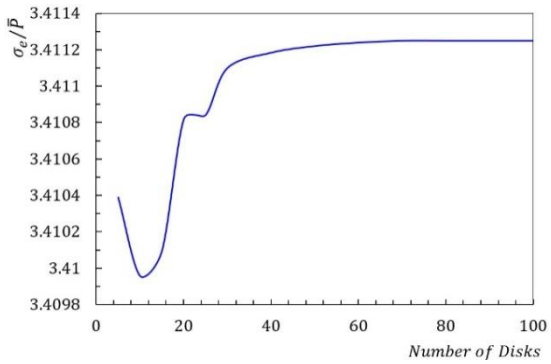

(b)

Fig. 4 Variation of normalized radial displacement and effective stress along the number of disk layers after 10000 hr of creeping in middle layer ($x = L/2$)

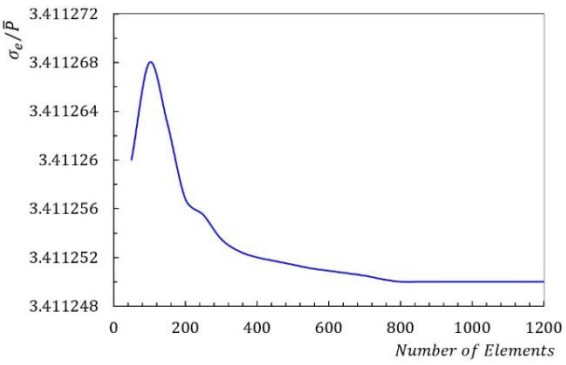

Fig. 5 Variation of normalized effective stress along the number of elements after 10000 hr of creeping in middle layer ($x = L/2$)

predicting creep stress responses of truncated cone. The geometrical characteristics of cone are assumed as a = 40 mm, b = 20 mm and L = 1000 mm. 304 L Austenitic Stainless Steel (304 L SS) is being used in this paper as material due to its excellent creep resistance. Type 304 L is an extra low-carbon variation of type 304 with 0.03% maximum carbon content that eliminates carbide precipitation due to welding. The following data for loading and material properties for type 304 L are used in this investigation (Tahami *et al*. 2010)

$$E = 179\ \text{GPa},\ \upsilon = 0.3,\ \alpha = 16.9\times10^{-6}\ ^{\circ}\text{C},$$
$$k_T = 16.2\ \text{W/m}^{\circ}\text{C},\ P_1 = 60\ \text{MPa},\ P_2 = 20\ \text{MPa},$$
$$A = 7.18\times10^{-43}\ \text{Pa}^{-n}\text{s}^{-1},\ n = 5.7278.$$

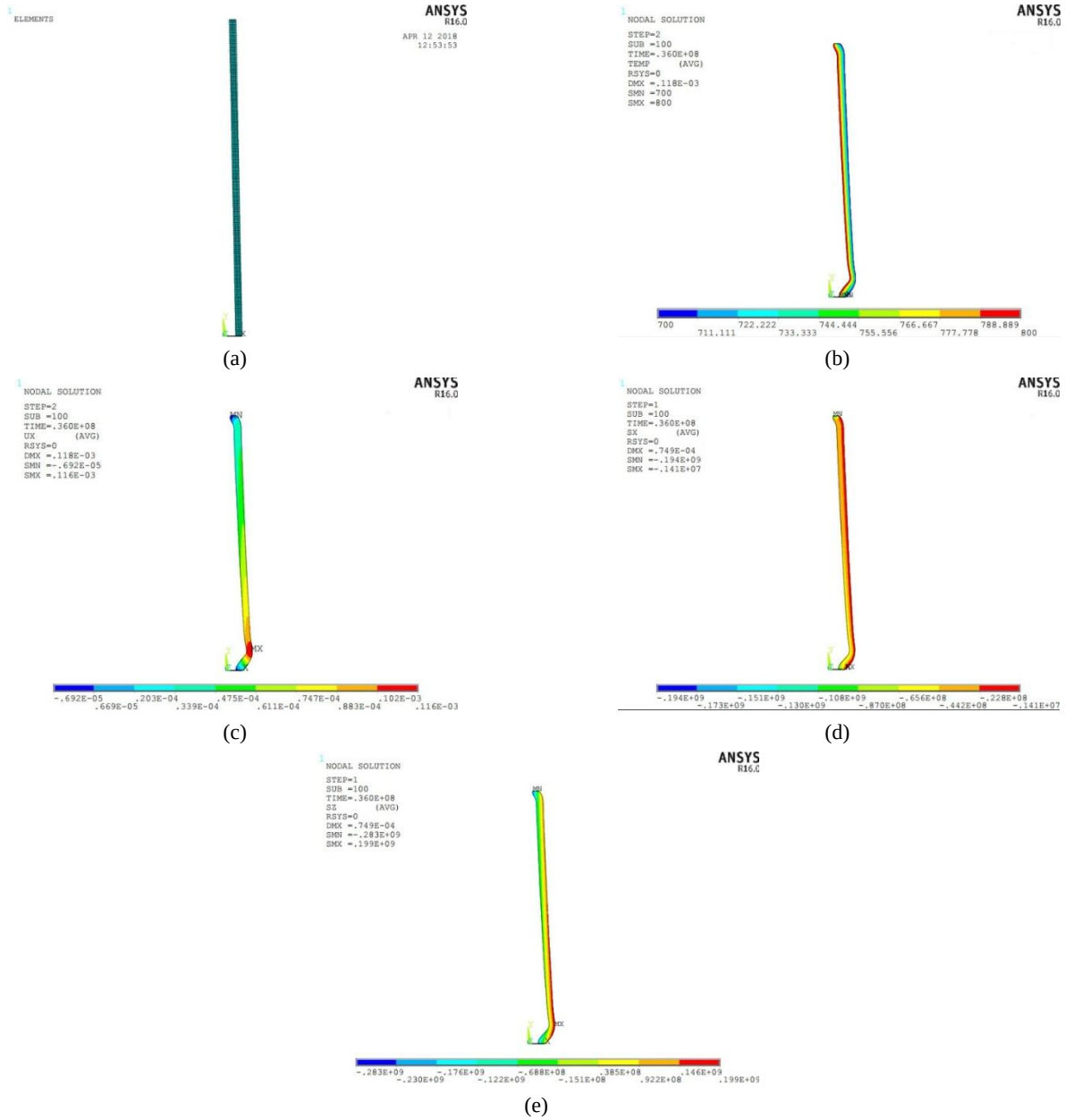

(a) (b) (c) (d) (e)

Fig. 6 Finite-element model for the truncated cone: (a) Finite-element mesh; (b) Temperature gradient; (c) Radial displacement; (d) Radial stress; (e) Circumferential stress distribution in the truncated cone after 10000 hr of creeping

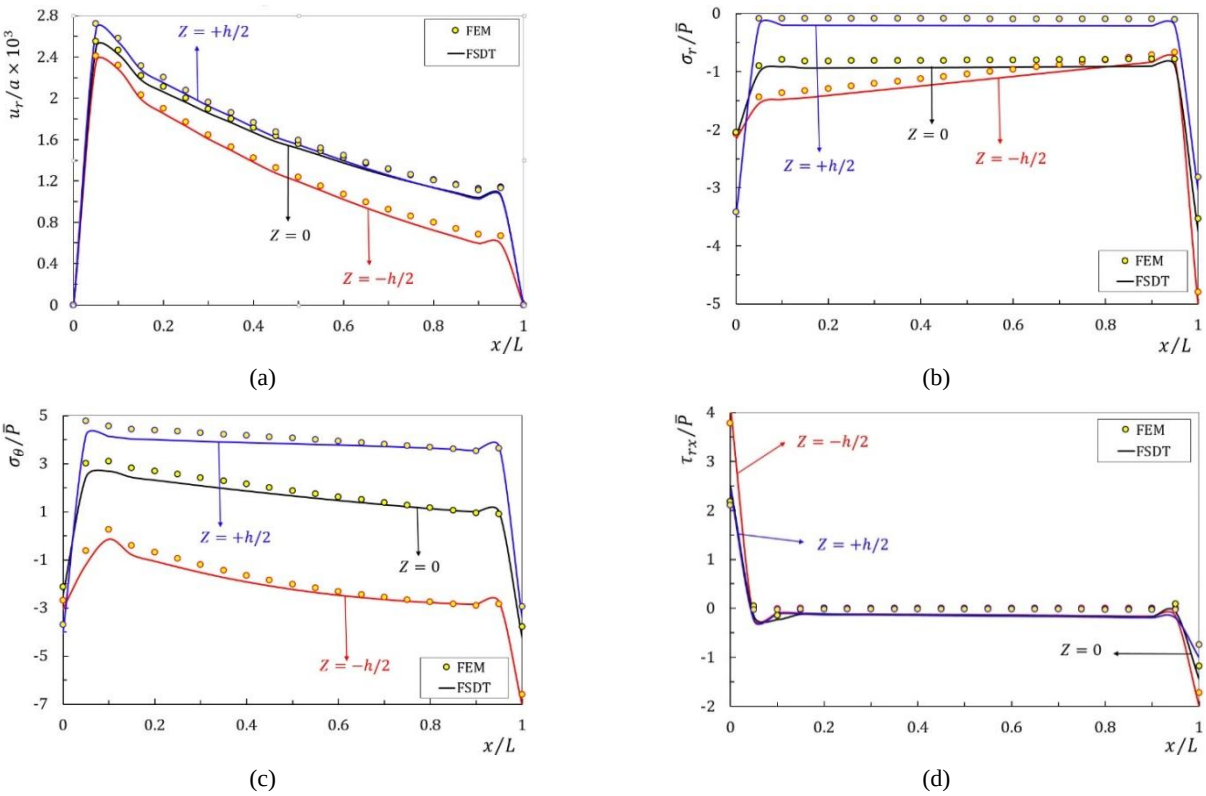

Fig. 7 Variation of normalized creep displacement and stresses along the dimensionless axial direction after 10000 hr of creeping in middle layer

Creep will occur in any metal subjected to a sustained load at a temperature slightly about its recrystallization temperature. At this temperature, the atoms become quite mobile. As a result, time-dependent alterations of the metal's structure occur. It is often stated that "elevated temperature" for creep behavior of a metal begins at about one-half the melting temperature T_m, of a metal (Bores and Schmidt 2003, Naumenko and Altenbach 2007). Therefore, in this study, the boundary conditions for temperature are taken as T_i = 800℃ and T_o = 700℃ (304L SS melting temperature range is 1399℃-1454℃). The results are presented in a non-dimensional form. In order to normalize stresses, we define the mean internal pressure parameter as follows

$$\bar{P} = \left(P_1 + P_2\right)/2 \tag{43}$$

The number of disk layers have significant effect on the results. In order to show the effectiveness of disk layers, variation of normalized radial displacement and effective stress along the number of disks is shown in Fig. 4(a) and (b). It could be observed that if the number of disk layers is more than 60, there will be no significant effect on radial displacement and effective stress and other results. In the present study, 80 disks are used.

For meshing of finite element model, it has been used of 800 elements. Fig. 5 illustrates a valid range for using number of elements in calculating the effective stress after 10000 hr of creeping in middle layer. It could be observed that if the number of elements is more than 800 elements, there will be no significant effect on effective stress.

In order to show the effectiveness and accuracy of the approach suggested here, a comparison between responses of the present theory and FEM can be made. In FEM, a thick truncated cone was modeled using ANSYS®. The PLANE 223 element in axisymmetric mode, which is an element with eight nodes with up to four degrees of freedom per each node, was used for discretization. There is a good agreement among numerical results based on FSDT and FEM. Fig. 6 illustrates the finite-element model is established with ANSYS® after 10000 hr of creeping.

In Fig. 7, displacement and stress distributions at different layers are obtained using multilayer method, and compared with the solutions of FEM, and are presented in the form of graphs. Fig. 7 show that the disk layer method based on FSDT has an acceptable amount of accuracy when one wants to obtain radial displacement, radial stress, circumferential stress, and shear stress.

Fig. 7(a) shows that the radial displacement at points away from the boundaries depends on radius and length. According to Fig. 7(a), the change in radial displacement in the lower boundary is greater than that of the upper boundary and the greatest radial displacement occurs in the outer surface (z = +h/2). It can be seen from Fig. 7(b) that, at points away from the boundaries, the absolute minimums of radial creep stress occur at the outer surface of the cone. Also Fig. 7(c) shows that, at points away from the boundaries the absolute maximums of circumferential creep stress occur at the outer surface. Fig. 7(d) shows the distribution of shear stress at different layers. The shear stress at points away from the boundaries at different layers

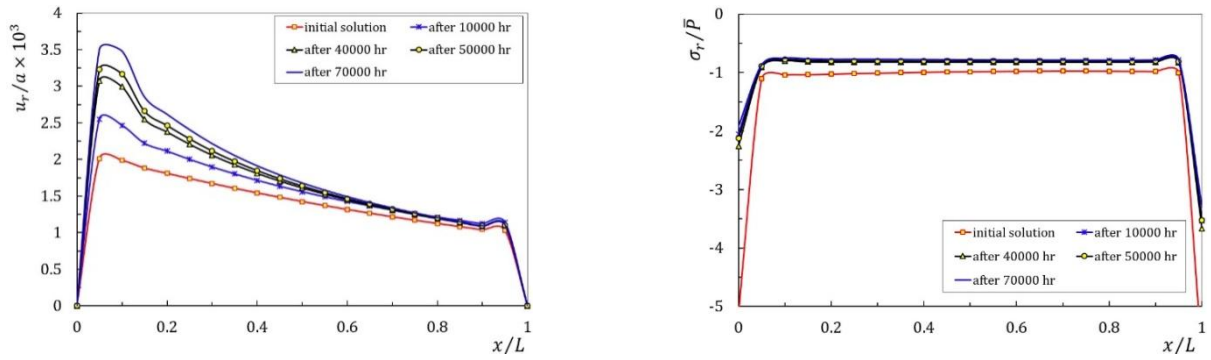

(a) (b)

Fig. 8 Variation of normalized radial displacement and radial stress along the dimensionless axial direction from initial solution at zero time up to 70000 hr

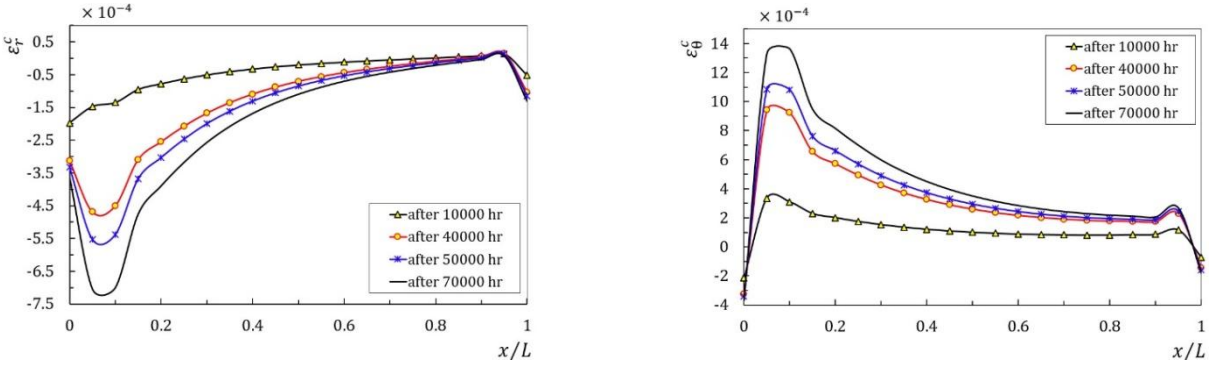

(a) (b)

Fig. 9 Variation of radial and circumferential creep strains along the dimensionless axial direction up to 70000 hr

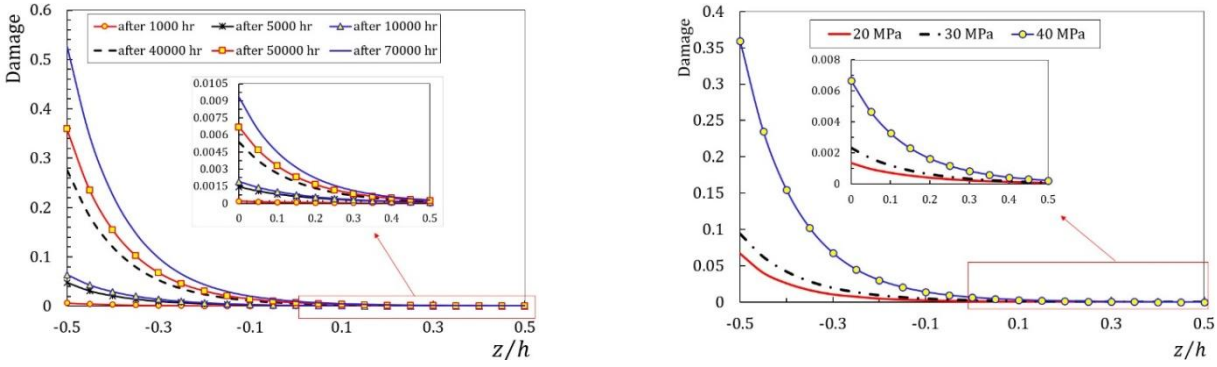

(a) (b)

Fig. 10 (a) Variation of creep damage along the dimensionless radial direction; (b) Effect of internal pressure on creep damage distribution after 50000 hr of creeping

is the same and trivial. However, at points near the boundaries, the stress is significant, especially in the outer surface, which is the greatest.

Histories of normalized radial displacement and radial stress from initial solution at zero time up to 70000 hr in middle layer are shown in Fig 8. It is clear from these figures that the absolute value of radial displacement increases with time during creep process of the truncated cone, but the absolute values of radial stress decreases.

Histories of radial and circumferential creep strains are plotted in Fig. 9. It could be observed that the change in radial and circumferential creep strains in the lower boundary is greater than that of the upper boundary. As far as the creep time increases, the absolute value of both radial and circumferential creep strains increase.

Creep damage and effect of internal pressure on creep damage histories are illustrated in Figs. 10(a) and (b). Figs. 11(a) and (b) also show the remaining life and effect of internal pressure on remaining life histories along the dimensionless radial direction of the truncated cone at $x = L/2$. Maximum damages and the minimum remaining lives are located at the inner surface of the truncated cone as

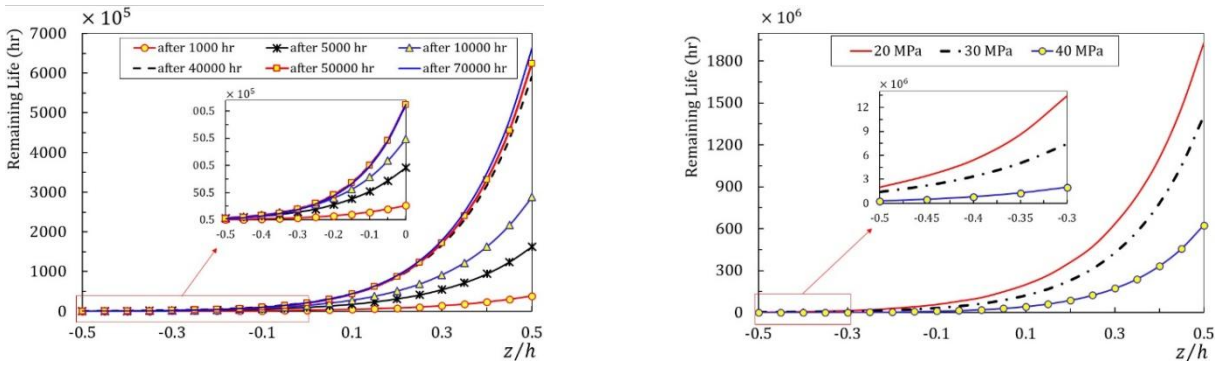

(a) (b)

Fig. 11 (a) Variation of remaining life along the dimensionless radial direction; (b) Effect of internal pressure on remaining life distribution after 50000 hr of creeping

illustrated in Figs. 10 and 11. It can be seen from Figs. 10(b) and 11(b) that with increasing internal pressure, creep damages increase and remaining lives decrease.

5. Conclusions

Creep response of isotropic thick-walled truncated conical shells subjected to the temperature gradient and internal non-uniform pressure made of 304 L austenitic stainless steel has been investigated in the present study by taking into account the creep behavior, as described by Norton's model. The governing equations are based on FSDT that accounts for the transverse shear. Using multilayered method, the thick conical shell is divided into disks with constant height. Considering continuity between layers and applying boundary conditions, the governing set of differential equations with constant coefficients are solved. The creep damage obtained by Robinson's linear life fraction damage rule and LMP is used to obtain creep remaining life assessment. The results obtained for stresses and displacement are compared with the solutions carried out through the FEM. Good agreement was found between the analytical solutions and the solutions carried out through the FEM.

General observations of this study could be summarized as follows:

- Shear deformation theory, is a popular model in structural analysis. In shear deformation theory, any changes in the axial direction of a thick shell as geometry parameters and boundary conditions, cause variable coefficients in the governing differential equations. The system of differential equations with variable coefficients can be changed to a set of differential equations with constant coefficients by multilayered method.
- The results show that the multilayered method based on FSDT has an acceptable amount of accuracy when one wants to obtain radial displacement, radial stress, circumferential stress, and shear stress.
- The maximum creep life is located at the outer surface of the cone where the minimum value of temperature is located.
- Increasing internal pressure have considerably increased creep damages and decreased the remaining life of the conical shell.

References

Abdelaziz, H.H., Meziane, M.A.A., Bousahla, A.A., Tounsi, A., Mahmoud, S.R. and Alwabli, A.S. (2017), "An efficient hyperbolic shear deformation theory for bending, buckling and free vibration of FGM sandwich plates with various boundary conditions", *Steel Compos. Struct., Int. J.*, **25**(6), 693-704.

Afshin, A., Nejad, M.Z. and Dastani, K. (2017), "Transient thermoelastic analysis of FGM rotating thick cylindrical pressure vessels under arbitrary boundary and initial conditions", *J. Comput. Appl. Mech.*, **48**(1), 15-26.

Ahmed, J.A. and Wahab, M.A. (2015), "Thermoelastic and creep analysis of a functionally graded rotating cylindrical vessel with internal heat generation", *World J. Eng.*, **12**(6), 517-532.

Altenbach, H., Gorash, Y. and Naumenko, K. (2008), "Steady-state creep of a pressurized thick cylinder in both the linear and the power law ranges", *Acta Mech.*, **195**(1-4), 263-274.

Bores, A.P. and Schmidt, R.J. (2003), *Advanced Mechanics of Materials*, John Wiley & Sons, Inc., New York, NY, USA.

Dai, H.-L. and Zheng, H.-Y. (2012), "Creep buckling and post-buckling analyses of a viscoelastic FGM cylindrical shell with initial deflection subjected to a uniform in-plane load", *J. Mech.*, **28**(2), 391-399.

Dehghan, M., Nejad, M.Z. and Moosaie, A. (2016), "Thermo-electro-elastic analysis of functionally graded piezoelectric shells of revolution: Governing equations and solutions for some simple cases", *Int. J. Eng. Sci.*, **104**, 34-61.

Eipakchi, H., Rahimi, G. and Esmaeilzadeh, K. (2003), "Closed form solution for displacements of thick cylinders with varying thickness subjected to non-uniform internal pressure", *Struct. Eng. Mech., Int. J.*, **16**(6), 731-748.

Fatehi, P. and Nejad, M.Z. (2014), "Effects of material gradients on onset of yield in FGM rotating thick cylindrical shells", *Int. J. Appl. Mech.*, **6**(4), Article Number: 1450038.

Fesharaki, J.J., Loghman, A., Yazdipoor, M. and Golabi, S. (2014), "Semi-analytical solution of time-dependent thermomechanical creep behavior of FGM hollow spheres", *Mech. Time-Depend. Mater.*, **18**(1), 41-53.

Foroutan, M., Moradi-Dastjerdi, R. and Sotoodeh-Bahreini, R. (2012), "Static analysis of FGM cylinders by a mesh-free method", *Steel Compos. Struct., Int. J.*, **12**(1), 1-11.

Ghannad, M. and Nejad, M.Z. (2010), "Elastic analysis of pressurized thick hollow cylindrical shells with clamped-

clamped ends", *Mechanika*, **5**(85), 11-18.
Ghannad, M. and Nejad, M.Z. (2013), "Elastic solution of pressurized clamped-clamped thick cylindrical shells made of functionally graded materials", *J. Theor. Appl. Mech.*, **51**(4), 1067-1079.
Ghannad, M., Nejad, M.Z. and Rahimi, G.H. (2009), "Elastic solution of axisymmetric thick truncated conical shells based on first-order shear deformation theory", *Mechanika*, **79**(5), 13-20.
Ghannad, M., Rahimi, G.H. and Nejad, M.Z. (2012a), "Determination of displacements and stresses in pressurized thick cylindrical shells with variable thickness using perturbation technique", *Mechanika*, **18**(1), 14-21.
Ghannad, M., Nejad, M.Z., Rahimi, G.H. and Sabouri, H. (2012b), "Elastic analysis of pressurized thick truncated conical shells made of functionally graded materials", *Struct. Eng. Mech., Int. J.*, **43**(1), 105-126.
Ghannad, M., Rahimi, G.H. and Nejad, M.Z. (2013), "Elastic analysis of pressurized thick cylindrical shells with variable thickness made of functionally graded materials", *Compos. Part B- Eng.*, **45**(1), 388-396.
Gharibi, M., Nejad, M.Z. and Hadi, A. (2017), "Elastic analysis of functionally graded rotating thick cylindrical pressure vessels with exponentially-varying properties using power series method of Frobenius", *J. Comput. Appl. Mech.*, **48**(1), 89-98.
Hachemi, H., Kaci, A., Houari, M.S.A., Bourada, M., Tounsi, A. and Mahmoud, S.R. (2017), "A new simple three-unknown shear deformation theory for bending analysis of FG plates resting on elastic foundations", *Steel Compos. Struct., Int. J.*, **25**(6), 717-726.
Jabbari, M., Nejad, M.Z. and Ghannad, M. (2015), "Thermo-elastic analysis of axially functionally graded rotating thick cylindrical pressure vessels with variable thickness under mechanical loading", *Int. J. Eng. Sci.*, **96**, 1-18.
Jabbari, M., Nejad, M.Z. and Ghannad, M. (2016), "Thermo-elastic analysis of axially functionally graded rotating thick truncated conical shells with varying thickness", *Compos. Part B- Eng.*, **96**, 20-34.
Jandaghian, A.A. and Rahmani, O. (2017), "Vibration analysis of FG nanobeams based on third-order shear deformation theory under various boundary conditions", *Steel Compos. Struct., Int. J.*, **25**(1), 67-78.
Kashkoli, M.D. and Nejad, M.Z. (2014), "Effect of heat flux on creep stresses of thick-walled cylindrical pressure vessels", *J. Appl. Res. Technol.*, **12**(3), 585-597.
Kashkoli, M.D. and Nejad, M.Z. (2015), "Time-dependent thermo-elastic creep analysis of thick-walled spherical pressure vessels made of functionally graded materials", *J. Theor. Appl. Mech.*, **53**(4), 1053-1065.
Kashkoli, M., Tahan, K.N. and Nejad, M.Z. (2017a), "Time-dependent creep analysis for life assessment of cylindrical vessels using first order shear deformation theory", *J. Mech.*, **33**(4), 461-474.
Kashkoli, M.D., Tahan, K.N. and Nejad, M.Z. (2017b), "Time-dependent thermomechanical creep behavior of FGM thick hollow cylindrical shells under non-uniform internal pressure", *Int. J. Appl. Mech.*, **9**(6), Article Number: 1750086.
Kashkoli, M.D., Tahan, K.N. and Nejad, M.Z. (2018), "Thermo-mechanical creep analysis of FGM thick cylindrical pressure vessels with variable thickness", *Int. J. Appl. Mech.*, **10**(1), Article Number: 1850008.
Larson, F.R. and Miller, J. (1952), *A Time-Temperature Relationship for Rupture and Creep Stresses*, Transaction ASME.
Loghman, A. and Moradi, M. (2013), "The analysis of time-dependent creep in FGPM thick walled sphere under electro-magneto-thermo-mechanical loadings", *Mech. Time-Depend. Mater.*, **17**(3), 315-329.
Loghman, A., Ghorbanpour Arani, A., Amir, S. and Vajedi, A. (2010), "Magnetothermoelastic creep analysis of functionally graded cylinders", *Int. J. Pres. Ves. Pip.*, **87**(7), 389-395.
Loghman, A., Ghorbanpour Arani, A. and Aleayoub, S. (2011), "Time-dependent creep stress redistribution analysis of thick-walled functionally graded spheres", *Mech. Time-Depend. Mater.*, **15**(4), 353-365.
Mazarei, Z., Nejad, M.Z. and Hadi, A. (2016), "Thermo-elasto-plastic analysis of thick-walled spherical pressure vessels made of functionally graded materials", *Int. J. Appl. Mech.*, **8**(4), Article Number: 1650054.
Mehditabar, A., Alashti, R.A. and Pashaei, M. (2014), "Magneto-thermo-elastic analysis of a functionally graded conical shell", *Steel Compos. Struct., Int. J.*, **16**(1), 77-96.
Naumenko, K. and Altenbach, H. (2007), *Modeling of Creep for Structural Analysis*, Springer Science & Business Media.
Nejad, M.Z. and Fatehi, P. (2015), "Exact elasto-plastic analysis of rotating thick-walled cylindrical pressure vessels made of functionally graded materials", *Int. J. Eng. Sci.*, **86**, 26-43.
Nejad, M.Z. and Kashkoli, M.D. (2014), "Time-dependent thermo-creep analysis of rotating FGM thick-walled cylindrical pressure vessels under heat flux", *Int. J. Eng. Sci.*, **82**, 222-237.
Nejad, M.Z., Jabbari, M. and Ghannad, M. (2014a), "A semi-analytical solution of thick truncated cones using matched asymptotic method and disk form multilayers", *Arch. Mech. Eng.*, **61**(3), 495-513.
Nejad, M.Z., Rastgoo, A. and Hadi, A. (2014b), "Exact elasto-plastic analysis of rotating disks made of functionally graded materials", *Int. J. Eng. Sci.*, **85**, 47-57.
Nejad, M.Z., Hoseini, Z., Niknejad, A. and Ghannad, M. (2015a), "Steady-state creep deformations and stresses in FGM rotating thick cylindrical pressure vessels", *J. Mech.*, **31**(1), 1-6.
Nejad, M.Z., Jabbari, M. and Ghannad, M. (2015b), "Elastic analysis of FGM rotating thick truncated conical shells with axially-varying properties under non-uniform pressure loading", *Compos. Struct.*, **122**, 561-569.
Nejad, M.Z., Jabbari, M. and Ghannad, M. (2017), "A general disk form formulation for thermo-elastic analysis of functionally graded thick shells of revolution with arbitrary curvature and variable thickness", *Acta Mech.*, **228**(1), 215-231.
Nobakhti, H. and Soltani, N. (2014), "Evaluating small punch test as accelerated creep test using Larson–Miller parameter", *Exp. Tech.*, **40**(2), 645-650.
Obata, Y. and Noda, N. (1994), "Steady thermal stresses in a hollow circular cylinder and a hollow sphere of a functionally gradient material", *J. Therm. Stress.*, **14**, 471-487.
Pankaj Thakur, D., Gupta, N. and Bir Singh, S. (2017), "Creep strain rates analysis in cylinder under temperature gradient materials by using Seth's theory", *Eng. Computat.*, **34**(3), 1020-1030.
Robinson, E.L. (1952), "Effect of temperature variation on the long-time rupture strength of steels", *Transaction ASME*, **74**(5), 777-781.
Sekkal, M., Fahsi, B., Tounsi, A. and Mahmoud, S.R. (2017), "A novel and simple higher order shear deformation theory for stability and vibration of functionally graded sandwich plate", *Steel Compos. Struct., Int. J.*, **25**(4), 389-401.
Singh, T. and Gupta, V. (2010), "Modeling steady state creep in functionally graded thick cylinder subjected to internal pressure", *J. Compos. Mater.*, **44**(11), 1317-1333.
Singh, T. and Gupta, V. (2014), "Analysis of steady state creep in whisker reinforced functionally graded thick cylinder subjected to internal pressure by considering residual stress", *Mech. Adv. Mater. Struct.*, **21**(5), 384-392.
Sofiyev, A.H. (2017), "The stability analysis of shear deformable FGM sandwich conical shells under the axial load", *Compos. Struct.*, **176**, 803-811.

Sofiyev, A.H. (2018a), "Application of the first order shear deformation theory to the solution of free vibration problem for laminated conical shells", *Compos. Struct*., **188**, 340-346.
Sofiyev, A.H. (2018b), "Application of the FOSDT to the solution of buckling problem of FGM sandwich conical shells under hydrostatic pressure", *Compos. Part B-Eng*., **144**, 88-98.
Sofiyev, A.H. and Aksogan, O. (2002), "The dynamic stability of a nonhomogeneous orthotropic elastic truncated conical shell under a time dependent external pressure", *Struct. Eng. Mech., Int. J*., **13**(3), 329-343.
Sofiyev, A.H. and Osmancelebioglu, E. (2017), "The free vibration of sandwich truncated conical shells containing functionally graded layers within the shear deformation theory", *Compos. Part B-Eng*., **120**, 197-211.
Sofiyev, A.H., Keskin, E.M., Erdem, H. and Zerin, Z. (2003), "Buckling of an orthotropic cylindrical thin shell with continuously varying thickness under a dynamic loading", *Indian J. Eng. Mater. Sci*., **10**(5), 365-370.
Sofiyev, A.H., Zerin, Z., Allahverdiev, B.P., Hui, D., Turan, F. and Erdem, H. (2017), "The dynamic instability of FG orthotropic conical shells within the SDT", *Steel Compos. Struct., Int. J*., **25**(5), 581-591.
Tahami, F.V., Sorkhabi, A.H.D. and Biglari, F.R. (2010), "Creep constitutive equations for cold-drawn 304L stainless steel", *Mat. Sci. Eng*: *A*, **527**(18), 4993-4999.
Van Dung, D. and Chan, D.Q. (2017), "Analytical investigation on mechanical buckling of FGM truncated conical shells reinforced by orthogonal stiffeners based on FSDT", *Compos. Struct*., **159**, 827-841.
Vlachoutsis, S. (1992), "Shear correction factors for plates and shells", *Int. J. Numer. Method. Eng*., **33**(7), 1537-1552.
Yang, Y. (2000), "Time-dependent stress analysis in functionally graded materials", *Int. J. Solids Struct*., **37**(51), 7593-7608.
You, L., Ou, H. and Zheng, Z. (2007), "Creep deformations and stresses in thick-walled cylindrical vessels of functionally graded materials subjected to internal pressure", *Compos. Struct*., **78**(2), 285-291.

CC

Appendix A

$$[B_1]=\begin{bmatrix} 0 & 0 & 0 & 0 \\ 0 & (1-\upsilon)\dfrac{h^3}{12}R & 0 & 0 \\ 0 & 0 & \mu hR & \dfrac{\mu h^3}{12} \\ 0 & 0 & \dfrac{\mu h^3}{12} & \dfrac{\mu h^3}{12}R \end{bmatrix} \tag{A1}$$

$$[B_2]=\begin{bmatrix} 0 & (1-\upsilon)\dfrac{h^3}{12} & 0 & 0 \\ (1-\upsilon)\dfrac{h^3}{12} & (1-\upsilon)\dfrac{h^2}{12}\left(3R\dfrac{dh}{dx}+h\dfrac{dR}{dx}\right) & -\mu hR & -(\mu-2\upsilon)\dfrac{h^3}{12} \\ 0 & \mu hR & \mu\left(R\dfrac{dh}{dx}+h\dfrac{dR}{dx}\right) & \dfrac{\mu h^2}{4}\dfrac{dh}{dx} \\ 0 & (\mu-2\upsilon)\dfrac{h^3}{12} & \dfrac{\mu h^2}{4}\dfrac{dh}{dx} & \dfrac{\mu h^2}{12}\left(3R\dfrac{dh}{dx}+h\dfrac{dR}{dx}\right) \end{bmatrix} \tag{A2}$$

$$[B_3]=\begin{bmatrix} (1-\upsilon)hR & 0 & \upsilon h & \upsilon hR \\ (1-\upsilon)\dfrac{h^2}{4}\dfrac{dh}{dx} & -\mu hR & 0 & \dfrac{\upsilon h^2}{2}\dfrac{dh}{dx} \\ -\upsilon h & \mu\left(R\dfrac{dh}{dx}+h\dfrac{dR}{dx}\right) & -(1-\upsilon)\alpha & -h+(1-\upsilon)\alpha R \\ -\upsilon hR & \dfrac{\mu h^2}{4}\dfrac{dh}{dx} & -h+(1-\upsilon)\alpha R & -(1-\upsilon)\alpha R^2 \end{bmatrix} \tag{A3}$$

$$\{F\}=\frac{1}{E\lambda}\begin{Bmatrix} -\int P_x\left(R-\dfrac{h}{2}\right)dx+E\lambda D_1(x)+C_0 \\ P_x\dfrac{h}{2}\left(R-\dfrac{h}{2}\right)+E\lambda\dfrac{dD_2(x)}{dx} \\ -P_z\left(R-\dfrac{h}{2}\right)-E\lambda D_3(x) \\ P_z\dfrac{h}{2}\left(R-\dfrac{h}{2}\right)-E\lambda\left[D_4(x)+D_5(x)\right] \end{Bmatrix} \tag{A4}$$

$$\begin{cases} \mu=\dfrac{5}{12}(1-2\upsilon) \\ \alpha=ln\left[\left(R+\dfrac{h}{2}\right)\Big/\left(R-\dfrac{h}{2}\right)\right] \end{cases} \tag{A5}$$

Also

$$\begin{cases} D_1(x)=R\int_{-\frac{h}{2}}^{\frac{h}{2}}\left[(1-\upsilon)\varepsilon_x^c+\upsilon\left(\varepsilon_\theta^c+\varepsilon_z^c\right)+(1+\upsilon)\alpha_T T\right](1+z/R)dz \\ D_2(x)=R\int_{-\frac{h}{2}}^{\frac{h}{2}}\left[(1-\upsilon)\varepsilon_x^c+\upsilon\left(\varepsilon_\theta^c+\varepsilon_z^c\right)+(1+\upsilon)\alpha_T T\right]z(1+z/R)dz \\ D_3(x)=\int_{-\frac{h}{2}}^{\frac{h}{2}}\left[(1-\upsilon)\varepsilon_\theta^c+\upsilon\left(\varepsilon_x^c+\varepsilon_z^c\right)+(1+\upsilon)\alpha_T T\right]dz \\ D_4(x)=\int_{-\frac{h}{2}}^{\frac{h}{2}}\left[(1-\upsilon)\varepsilon_\theta^c+\upsilon\left(\varepsilon_x^c+\varepsilon_z^c\right)+(1+\upsilon)\alpha_T T\right]zdz \\ D_5(x)=R\int_{-\frac{h}{2}}^{\frac{h}{2}}\left[(1-\upsilon)\varepsilon_z^c+\upsilon\left(\varepsilon_x^c+\varepsilon_\theta^c\right)+(1+\upsilon)\alpha_T T\right](1+z/R)dz \end{cases} \tag{A6}$$

Appendix B

General thermal boundary conditions are

$$\begin{cases} C_{11}{}^{[k]}T^{[k]}\Big|_{z=-\frac{h^{[k]}}{2}} + C_{12}{}^{[k]}\dfrac{dT^{[k]}}{dz}\Big|_{z=-\frac{h^{[k]}}{2}} = f_1^{[k]} \\ C_{21}{}^{[k]}T^{[k]}\Big|_{z=\frac{h^{[k]}}{2}} + C_{22}{}^{[k]}\dfrac{dT^{[k]}}{dz}\Big|_{z=\frac{h^{[k]}}{2}} = f_2^{[k]} \end{cases} \tag{B1}$$

where $C_{ij}^{[k]}(i=1,2;\ j=1,2)$ are constants which depend on the thermal conductivity and the thermal convection. $f_1^{[k]}$ and $f_2^{[k]}$ are constants which are evaluated at the inner and outer radii, respectively. By exerting the boundary conditions for the temperature gradient distribution, we have

$$\begin{cases} g_1^{[k]} = \dfrac{\left(C_{21}{}^{[k]} f^{[k]}{}_1 - C_{11}{}^{[k]} f_2^{[k]}\right)}{C_{11}{}^{[k]}C_{21}{}^{[k]}\, ln\left(\dfrac{R^{[k]}+h^{[k]}/2}{R^{[k]}-h^{[k]}/2}\right) + \dfrac{C_{11}{}^{[k]}C_{22}{}^{[k]}}{R^{[k]}+h^{[k]}/2} - \dfrac{C_{12}{}^{[k]}C_{21}{}^{[k]}}{R^{[k]}-h^{[k]}/2}} \\ g_2^{[k]} = \dfrac{C_{21}{}^{[k]}\, ln\left(R^{[k]}+h^{[k]}/2\right) f_1^{[k]} - C_{11}{}^{[k]}\, ln\left(R^{[k]}+h^{[k]}/2\right) f_2^{[k]} + \dfrac{C_{22}{}^{[k]} f^{[k]}{}_1}{R^{[k]}+h^{[k]}/2} - \dfrac{C_{12}{}^{[k]} f_2^{[k]}}{R^{[k]}-h^{[k]}/2}}{C_{11}{}^{[k]}C_{21}{}^{[k]}\, ln\left(\dfrac{R^{[k]}+h^{[k]}/2}{R^{[k]}-h^{[k]}/2}\right) + \dfrac{C_{11}{}^{[k]}C_{22}{}^{[k]}}{R^{[k]}+h^{[k]}/2} - \dfrac{C_{12}{}^{[k]}C_{21}{}^{[k]}}{R^{[k]}-h^{[k]}/2}} \end{cases} \tag{B1}$$

In the present study, constants are defined by

$$\begin{cases} C_{11}{}^{[k]} = 1, C_{12}{}^{[k]} = 0, f_1^{[k]} = T_i \\ C_{21}{}^{[k]} = 1, C_{22}{}^{[k]} = 0, f_2^{[k]} = T_o \end{cases} \tag{B1}$$

Appendix C

$$\{F_c\} = \left\{ E_1(x) + \frac{D_0}{E\lambda} \quad \frac{dE_2(x)}{dx} \quad -E_3(x) \quad -E_4(x) - E_5(x) \right\}^T \tag{C1}$$

$$\begin{cases} E_1(x) = R\int_{-\frac{h}{2}}^{\frac{h}{2}} \left[(1-\upsilon)\dot{\varepsilon}_x^c + \upsilon\left(\dot{\varepsilon}_\theta^c + \dot{\varepsilon}_z^c\right) \right](1+z/R)dz \\ E_2(x) = R\int_{-\frac{h}{2}}^{\frac{h}{2}} \left[(1-\upsilon)\dot{\varepsilon}_x^c + \upsilon\left(\dot{\varepsilon}_\theta^c + \dot{\varepsilon}_z^c\right) \right] z(1+z/R)dz \\ E_3(x) = \int_{-\frac{h}{2}}^{\frac{h}{2}} \left[(1-\upsilon)\dot{\varepsilon}_\theta^c + \upsilon\left(\dot{\varepsilon}_x^c + \dot{\varepsilon}_z^c\right) \right] dz \\ E_4(x) = \int_{-\frac{h}{2}}^{\frac{h}{2}} \left[(1-\upsilon)\dot{\varepsilon}_\theta^c + \upsilon\left(\dot{\varepsilon}_x^c + \dot{\varepsilon}_z^c\right) \right] z dz \\ E_5(x) = R\int_{-\frac{h}{2}}^{\frac{h}{2}} \left[(1-\upsilon)\dot{\varepsilon}_z^c + \upsilon\left(\dot{\varepsilon}_x^c + \dot{\varepsilon}_\theta^c\right) \right](1+z/R)\, dz \end{cases} \tag{C2}$$